Available online at www.sciencedirect.com
SCIENCE DIRECT®
Journal of Sound and Vibration 283 (2005) 153–172
JOURNAL OF SOUND AND VIBRATION
www.elsevier.com/locate/jsvi

Hydroelastic vibration of a circular plate submerged in a bounded compressible fluid

Kyeong-Hoon Jeong[a,*], Kwi-Ja Kim[b]

[a] *Mechanical Engineering Division, Korea Atomic Energy Research Institute, Yuseong, Daejeon 305-600, Republic of Korea*
[b] *Mechanical Engineering Department, Chungnam National University, Yuseong, Daejeon 305-764, Republic of Korea*

Received 8 September 2003; received in revised form 3 February 2004; accepted 2 April 2004
Available online 30 November 2004

Abstract

An analytical method for the linear free vibration of a circular plate submerged in a fluid was developed by the Rayleigh–Ritz method based on the Fourier–Bessel series expansion. It is assumed that the plate is clamped at an offcenter location of a rigid cylindrical container and the fluid bisected by the plate in the container is non-viscous and compressible. Since a combination of the dry modal functions of the circular plate can approximate the wet vibration modes, the functions were used to form a set of linearly independent functions of the Rayleigh–Ritz method. It was found that the theoretical results could predict well the fluid-coupled natural frequencies with excellent accuracy compared with the finite element analysis results. The effects of the fluid compressibility and the offcenter distance on the natural frequencies were also observed.

1. Introduction

This paper deals with the hydroelastic vibration of a circular plate submerged in a bounded compressible fluid. The circular plates can be used as compartments of a fuel tank or as the displacers in a nuclear reactor. Therefore, the purpose of this paper is to develop a theoretical method for hydroelastic behavior of a circular plate in contact with water. Free vibration of plates

*Corresponding author. Tel.: +82 42 868 8792.
E-mail address: khjeong@kaeri.re.kr (K.-H. Jeong).

0022-460X/$ - see front matter © 2004 Elsevier Ltd. All rights reserved.
doi:10.1016/j.jsv.2004.04.029

in contact with fluid has been studied recently. Kwak [1] and Kwak and Kim [2] studied the free vibrations of a circular plate resting on a free liquid surface for axisymmetric modes and the general case, respectively. They considered the unbounded fluid domain in the radial direction and also introduced the non-dimensionalized added virtual mass incremental (NAVMI) factors in order to estimate the fluid effect on the individual natural frequency of the fluid–structure coupled system. The effect of fluid depth under the free-edge circular plate was theoretically and experimentally investigated by Kwak and Han [3], and Amabili [4] analyzed the effect of the finite fluid depth above the baffled plate. Amabili and Kwak [5] have re-analyzed the same problem by using the Rayleigh–Ritz method based on the Hankel transformation and they [6] extended this study to the effect of free surface waves. Chiba [7] obtained exact solutions for the circular elastic bottom plate in a cylindrical rigid tank filled with fluid. The elastic bottom plate was supported by an elastic foundation and the free surface of the fluid was considered. Bauer [8] analytically determined the coupled natural frequencies of an ideal fluid in a circular cylindrical container with the fluid surface covered by a flexible membrane cover or an elastic plate. Amabili et al. [9] experimentally investigated the free vibration of a circular plate immersed in water and they also detected the difference between the corresponding mode shapes in air and in water. Cheung and Zhou [10] solved the vibration of a circular plate resting on a sloshing fluid surface by using the Galerkin method and the fluid domain was assumed to be limited by a rigid cylinder and a rigid flat bottom. Jeong [11] studied the free vibration of two identical circular plates coupled with a radially bounded fluid. In spite of the various previous researches on the circular plate in contact with a fluid, few studies on a circular plate in contact with a compressible fluid have been performed. Moreover, up to now, there was no effort to investigate the offcenter effect of a plate submerged in a rigid container. Also, for the hydroelastic vibration of a circular plate, few studies have been found on how much error can be produced owing to the incompressible fluid assumption for the water.

This paper is concerned with the coupling effect of fluid on the free vibration characteristics of a single circular plate supported by a rigid container filled with a compressible and frictionless fluid. The plate is clamped along the edge of the plate and bisects the fluid into two regions. The natural frequencies of the fluid-coupled system are obtained by using the Rayleigh–Ritz method and they are verified by using the finite element analysis. The normalized natural frequencies are plotted for the offcenter distance of the plate in order to estimate the relative added mass effect of the fluid on each vibration mode of the plate. Investigated are the effects of the fluid compressibility and the offcenter distance on the coupled natural frequency.

2. Theoretical background

2.1. Formulation for a circular plate

Fig. 1 represents a circular plate submerged in a fluid-filled rigid container, where R and h ($\ll R$) represent the radius and thickness of the circular plate, respectively. The following assumptions are made for a formulation: (a) the fluid motion is small; (b) the fluid is compressible, inviscid and irrotational; (c) the circular plate is made of linearly elastic, homogeneous, and isotropic material; and (d) the shear deformation and rotary inertia are negligible. The equation of motion for a

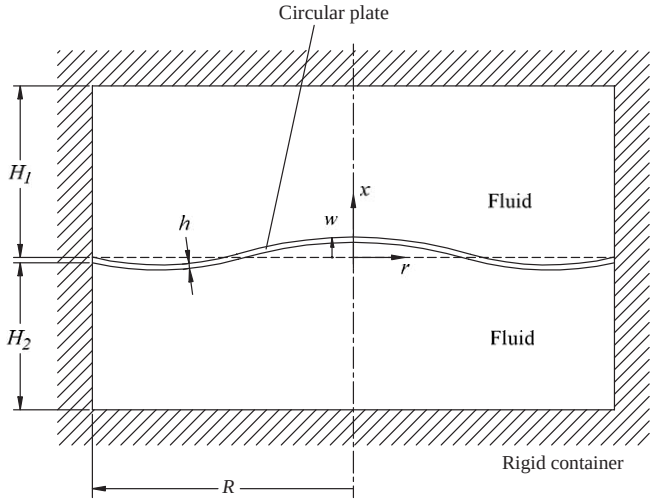

Fig. 1. A circular plate submerged in a rigid cylindrical container filled with a compressible fluid.

transverse displacement, w, of the circular plate is

$$D\nabla^4 w + \rho h w_{,tt} = p_u + p_l, \tag{1}$$

where p_u and p_l are the hydrodynamic pressures on the upper and lower surfaces of the plate, and $D = Eh^3/12(1-\mu^2)$ is the flexural rigidity of the circular plate; ρ, μ and E are the density, Poisson's ratio, and Young's modulus of the plate, respectively. The comma in the equation denotes a partial derivative with respect to the corresponding variable and t is time. In addition, ∇^4 in Eq. (1) represents the bi-harmonic operator in the polar coordinates r and θ. For the arbitrary nodal diameter n ($n = 0, 1, 2, \ldots$), the solution of Eq. (1) can be written in the form of

$$w(r,\theta,t) = w(r,\theta)\exp(\mathrm{i}\omega t) = \cos(n\theta)\sum_{m=1}^{M} q_m W_{nm}(r)\exp(\mathrm{i}\omega t), \tag{2}$$

where, $\mathrm{i} = \sqrt{-1}$ and ω is the fluid-coupled natural frequency of the plate. In order to find the mode shapes and natural frequencies of the plate in contact with the fluid, the Rayleigh–Ritz method is applied. Therefore, each wet mode shape can be expanded in a series by using a finite number of an admissible function $W_{nm}(r)$ ($m = 0, 1, 2, \ldots, M$) and the appropriate unknown coefficients q_m. The admissible function $W_{nm}(r)$ can be assumed as the dry eigen functions of the plate which satisfies the boundary condition along the plate edge. So, m represents the number of nodal circles of the dry plate, or the number of expanding terms for the radial modal function in the wet modes. For the clamped boundary condition of the plate, the displacement must be zero along the plate edge, that is, $W_{nm} = 0$ at $r = R$. Therefore, the modal displacement of Eq. (2) will be reduced to

$$W_{nm}(r) = J_n(\lambda_{nm} r) - J_n(\lambda_{nm} R) I_n(\lambda_{nm} r)/I_n(\lambda_{nm} R). \tag{3}$$

The frequency parameter for the plate in air, λ_{nm}, can be obtained using Eq. (3) which must satisfy the other geometric boundary condition, that is, the slope along the plate edge must be

zero, or $dW_{nm}(r)/dr = 0$ at $r = R$:

$$J_n(\lambda_{nm}R)I_{n+1}(\lambda_{nm}R) + J_{n+1}(\lambda_{nm}R)I_n(\lambda_{nm}R) = 0. \tag{4}$$

2.2. Velocity potentials

The fluid contained in a cylindrical rigid container is bisected into two regions; an upper and lower fluid region by the circular plate as shown in Fig. 1. The oscillatory fluid flow for each region can be described using the velocity potential in the cylindrical coordinates. The facing sides of the circular plate are contacted with the inviscid and compressible fluid. The fluid movement induced by plate vibration should satisfy the Helmholz equation:

$$\nabla^2\Phi_j(x, r, \theta, r) = \Phi_j(x, r, \theta, t)_{,tt}/c^2, \quad j = 1, 2, \tag{5}$$

where c is the sound speed in the fluid medium. The upper fluid is referred to with a subscript "1" while the lower fluid is denoted by a subscript "2". When the harmonic time function is assumed, the velocity function Φ_j can be separated with respect to x in terms of the displacement potential function, $\phi_j(r, \theta)$:

$$\Phi_j(x, r, \theta, t) = i\omega\phi_j(r, \theta, x)\exp(i\omega t) = i\omega\phi_j(r, \theta)\, f_j(x)\exp(i\omega t). \tag{6}$$

The first derivative of ϕ_j indicates the dynamic deformation of the fluid with respect to the corresponding direction. Insertion of Eq. (6) into Eq. (5) gives the two differential equations

$$\frac{\phi_j(r, \theta)_{,rr} + (1/r)\phi_j(r, \theta)_{,r} + (1/r^2)\phi_j(r, \theta)_{,\theta\theta} + (\omega^2/c^2)\phi_j(r, \theta)}{\phi_j(r, \theta)} = -\frac{f_j(x)_{,xx}}{f_j(x)} = -\alpha_{ns}^2. \tag{7}$$

Since the displacement potential at $r = 0$ must be finite, the general solution of Eq. (7) is given by

$$\phi_j(r, \theta, x) = \cos(n\theta)\sum_{s=1}^{\infty} J_n(\beta_{ns}r)\{E_{nsj}\sinh(\alpha_{ns}x) + F_{nsj}\cosh(\alpha_{ns}x)\}, \tag{8}$$

where

$$\beta_{ns}^2 = \alpha_{ns}^2 + (\omega/c)^2. \tag{9}$$

The radial displacement of the fluid must be zero at $r = R$, that is, Eqs. 15(a) and 15(b) should be satisfied. Therefore, the positive coefficient, β_{ns} can be determined by the following transcendental equation for every s and n:

$$J_n'(\beta_{ns}R) = 0. \tag{10}$$

When it is assumed that all the cylindrical container walls are rigid and the plate thickness is negligible compared with the container height, the displacement potential must satisfy the boundary conditions for the fluid:

$$\frac{\partial\phi_1(r, \theta, H_1)}{\partial x} = 0 \quad \text{for the upper fluid,} \tag{11}$$

$$\frac{\partial\phi_2(r, \theta, -H_2)}{\partial x} = 0 \quad \text{for the lower fluid,} \tag{12}$$

$$\frac{\partial\phi_1(R,\theta,x)}{\partial r}=\frac{\partial\phi_2(R,\theta,x)}{\partial r}=0 \quad \text{for the upper and lower fluids.} \tag{13}$$

Now the displacement potential for the upper and lower fluid regions can be rewritten by applying Eq. (8) to the boundary condition of Eqs. (11) and (12);

$$\phi_1(r,\theta,x)=\cos(n\theta)\sum_{s=1}^{\infty}E_{ns1}J_n(\beta_{ns}r)\left\{\sinh(\alpha_{ns}x)-\frac{\cosh(\alpha_{ns}x)}{\tanh(\alpha_{ns}H_1)}\right\}, \tag{14a}$$

$$\phi_2(r,\theta,x)=\cos(n\theta)\sum_{s=1}^{\infty}E_{ns2}J_n(\beta_{ns}r)\left\{\sinh(\alpha_{ns}x)+\frac{\cosh(\alpha_{ns}x)}{\tanh(\alpha_{ns}H_2)}\right\}. \tag{14b}$$

2.3. Method of solution

In order to determine the unknown coefficients E_{ns1} and E_{ns2} of fluid motion in Eqs. (14a) and (14b), the compatibility conditions at the interface of the upper and lower fluids in contact with the plate are used. Since the plate thickness is negligible compared with the container height, the compatibility conditions at the fluid interface with the plate yield:

$$w(r,\theta)=\left.\frac{\partial\phi_1}{\partial x}\right|_{x=0}, \tag{15a}$$

$$w(r,\theta)=\left.\frac{\partial\phi_2}{\partial x}\right|_{x=0}. \tag{15b}$$

The relationships can be obtained by substituting Eqs. (2), (3) and (14a,b) into Eqs. (15a,b).

$$\sum_{m=1}^{M}q_m\left[J_n(\lambda_{nm}r)-I_n(\lambda_{nm}r)\frac{J_n(\lambda_{nm}R)}{I_n(\lambda_{nm}R)}\right]=\sum_{s=1}^{\infty}E_{ns1}\alpha_{ns}J_n(\beta_{ns}r), \tag{16a}$$

$$\sum_{m=1}^{M}q_m\left[J_n(\lambda_{nm}r)-I_n(\lambda_{nm}r)\frac{J_n(\lambda_{nm}R)}{I_n(\lambda_{nm}R)}\right]=\sum_{s=1}^{\infty}E_{ns2}\alpha_{ns}J_n(\beta_{ns}r). \tag{16b}$$

Expanding $J_n(\lambda_{nm}r)$ and $I_n(\lambda_{nm}r)$ of Eqs. (16a,b) into the Bessel–Fourier series [8,12] will give

$$J_o(\lambda_{om}r)=\sum_{s=1}^{\infty}a_{oms}J_o(\beta_{os}r), \quad I_o(\lambda_{om}r)=\sum_{s=1}^{\infty}b_{oms}J_o(\beta_{os}r), \tag{17a,b}$$

$$J_n(\lambda_{nm}r)=\sum_{s=1}^{\infty}a_{nms}J_n(\beta_{ns}r), \quad I_n(\lambda_{nm}r)=\sum_{s=1}^{\infty}b_{nms}J_n(\beta_{ns}r), \tag{17c,d}$$

where

$$a_{oms} = \frac{-2(\lambda_{om}R)J_1(\lambda_{om}R)}{[(\beta_{os}R)^2 - (\lambda_{om}R)^2]J_o(\beta_{os}R)},$$

$$b_{oms} = \frac{2(\lambda_{om}R)I_1(\lambda_{om}R)}{[(\beta_{os}R)^2 + (\lambda_{om}R)^2]J_o(\beta_{os}R)} \quad \text{for } n = 0, \tag{18a, b}$$

$$a_{nms} = \frac{2(\beta_{ns}R)^2(\lambda_{nm}R)J'_n(\lambda_{nm}R)}{[(\beta_{ns}R)^2 - n^2][(\beta_{ns}R)^2 - (\lambda_{nm}R)^2]J_n(\beta_{ns}R)},$$

$$b_{nms} = \frac{2(\beta_{ns}R)^2(\lambda_{nm}R)I'_n(\lambda_{nm}R)}{[(\beta_{ns}R)^2 - n^2][(\beta_{ns}R)^2 + (\lambda_{nm}R)^2]J_n(\beta_{ns}R)} \quad \text{for } n>0. \tag{18c,d}$$

Therefore, the displacement potentials can be written in terms of the coefficient q_m instead of the unknown coefficients E_{ns1} and E_{ns2} by the arrangement of Eqs. (16a,b) and (17a–d).

For $n = 0$,

$$\phi_1(r,\theta,x) = \sum_{m=1}^{M} q_m \sum_{s=1}^{\infty} \Lambda_{oms} J_o(\beta_{os}r)\left\{\sinh(\alpha_{os}x) - \frac{\cosh(\alpha_{os}x)}{\tanh(\alpha_{os}H_1)}\right\}, \tag{19a}$$

$$\phi_2(r,\theta,x) = \sum_{m=1}^{M} q_m \sum_{s=1}^{\infty} \Lambda_{oms} J_o(\beta_{os}r)\left\{\sinh(\alpha_{os}x) + \frac{\cosh(\alpha_{os}x)}{\tanh(\alpha_{os}H_2)}\right\}, \tag{19b}$$

for $n>0$,

$$\phi_1(r,\theta,x) = \cos(n\theta) \sum_{m=1}^{M} q_m \sum_{s=1}^{\infty} \Lambda_{nms} J_n(\beta_{ns}r)\left\{\sinh(\alpha_{ns}x) - \frac{\cosh(\alpha_{ns}x)}{\tanh(\alpha_{ns}H_1)}\right\}, \tag{19c}$$

$$\phi_2(r,\theta,x) = \cos(n\theta) \sum_{m=1}^{M} q_m \sum_{s=1}^{\infty} \Lambda_{nms} J_n(\beta_{ns}r)\left\{\sinh(\alpha_{ns}x) + \frac{\cosh(\alpha_{ns}x)}{\tanh(\alpha_{ns}H_2)}\right\}, \tag{19d}$$

where

$$\Lambda_{oms} = \frac{4(\lambda_{om}R)^3 J_1(\lambda_{om}R)}{\alpha_{os}[(\lambda_{om}R)^4 - (\beta_{os}R)^4]J_o(\beta_{os}R)}, \tag{20a}$$

$$\Lambda_{nms} = \frac{4(\beta_{ns}R)^2(\lambda_{nm}R)^3 J'_n(\lambda_{nm}R)}{\alpha_{ns}[(\beta_{ns}R)^2 - n^2][(\beta_{ns}R)^4 - (\lambda_{nm}R)^4]J_n(\beta_{ns}R)}. \tag{20b}$$

Since gravity is neglected, it is useful to introduce the Rayleigh quotient to calculate the fluid-coupled natural frequencies of the circular plate submerged in the compressible fluid as suggested by Zhu [13] and Amabili [14]:

$$\omega^2 = \frac{V_d + V_F}{T_p^* + T_F^*}, \tag{21}$$

where V_d and V_F are the potential energies of the plate and the fluid, respectively. The reference kinetic energies of the plate and the fluid are denoted by T_p^* and T_F^*, respectively. In order to perform the numerical calculations for each fixed n value, a sufficiently large finite M number of terms must be considered in all the previous sums of expanding the term, m. For this purpose, a vector $\mathbf{q}$ of the unknown parameters is introduced:

$$\mathbf{q} = \{q_1 \quad q_2 \quad q_3 \quad \cdots \quad q_M\}^{\mathrm{T}}. \tag{22}$$

In the case of the compressible fluid, the work of the structural displacements on the fluid–structure interface is transformed into the potential energy of the fluid. The maximum potential energy stored in the compressible fluid is given by

$$V_F = \tfrac{1}{2}\rho_o c^2 \sum_{j=1}^{2} \left[\int_{V_j} \nabla^2\phi_j \nabla^2\phi_j \, \mathrm{d}V_j \right], \tag{23}$$

where V_j $(j = 1, 2)$ means the volume of the fluid domains, and ρ_o is the mass density of the fluid. The total fluid potential energy can be transformed by substituting Eqs. (5) and (6) into Eq. (23).

$$V_F = \tfrac{\rho_o \omega^2}{2} \sum_{j=1}^{2} \left[\int_{V_j} \phi_j \nabla^2\phi_j \, \mathrm{d}V_j \right]. \tag{24}$$

The reference kinetic energy of the contained fluids is given as

$$T_F^* = \tfrac{1}{2}\rho_o \sum_{j=1}^{2} \left[\int_{V_j} \nabla\phi_j \nabla\phi_j \, \mathrm{d}V_j \right], \tag{25}$$

The fluid-coupled natural frequency of Eq. (21) can be obtained by adding up Eqs. (24) and (25).

$$\omega^2 = \frac{V_d}{T_p^* + Q_F^*}, \tag{26}$$

where

$$Q_F^* = \tfrac{1}{2}\rho_o \sum_{j=1}^{2} \left[\int_{V_j} (\nabla\phi_j \cdot \nabla\phi_j + \phi_j \nabla^2\phi_j) \, \mathrm{d}V_j \right]. \tag{27}$$

From the Green's theorem for the displacement potentials,

$$\int_{V_j} (\nabla\phi_j \nabla\phi_j + \phi_j \nabla^2\phi_j) \, \mathrm{d}V_j = \int_{S_j} \phi_j \frac{\partial\phi_j}{\partial p} \, \mathrm{d}S_j, \tag{28}$$

where p is the positive direction outward to the fluid domain and S_j $(j = 1, 2)$ indicates the fluid surfaces. The fluid energy term Q_F^* including the fluid kinetic and potential energies can be

evaluated from its surface motion by using Eq. (28).

$$Q_F^* = \tfrac{1}{2}\rho_o \int_0^{2\pi}\int_0^R \left[\phi_1(r,\theta,x)\,\frac{\partial\phi_1(r,\theta,x)}{\partial x}\right]_{x=H_1} r\,\mathrm{d}r\,\mathrm{d}\theta + \tfrac{1}{2}\rho_o \int_0^{2\pi}\int_0^R \left[\phi_2(r,\theta,x)\,\frac{\partial\phi_2(r,\theta,x)}{\partial x}\right]_{x=H_2} r\,\mathrm{d}r\,\mathrm{d}\theta. \tag{29}$$

Application of Eqs. (15a,b) to Eq. (29) reduces to Eq. (30a):

$$Q_F^* = -\tfrac{1}{2}\kappa_\theta\rho_o q_m\left(\int_0^R W_{nm}(r)\xi_1(r,H_1)r\,\mathrm{d}r + \int_0^R W_{nm}(r)\xi_2(r,H_2)r\,\mathrm{d}r\right), \tag{30a}$$

where

$$\phi_j(r,\theta,x) = \xi_j(r,x)\cos(n\theta), \tag{30b}$$

$$\kappa_\theta = \begin{cases} 2\pi & \text{for } n=0, \\ \pi & \text{for } n>0. \end{cases} \tag{30c}$$

Now, the insertion of Eqs. (2), (3), (30b) and (19a–d) into Eq. (30a) gives the total fluid energy;

$$Q_F^* = \kappa_\theta \mathbf{q}^{\mathrm{T}}\mathbf{G}\mathbf{q}, \tag{31}$$

where the $M \times M$ symmetric matrix, $\mathbf{G}$ for the fixed n is calculated by Eqs. (14a,b) and (17a–d).

$$G_{ik} = 4R^3\rho_o \sum_{s=1}^{\infty} \frac{\Psi_{is}\Psi_{ks}\{\coth(\alpha_{os}H_1)+\coth(\alpha_{os}H_2)\}}{(\alpha_{os}R)} \quad \text{for } n=0, \tag{32a}$$

$$G_{ik} = 4R^3\rho_o \sum_{s=1}^{\infty} \frac{(\beta_{ns}R)^2\Psi_{is}\Psi_{ks}[\coth(\alpha_{ns}H_1)+\coth(\alpha_{ns}H_2)]}{(\alpha_{ns}R)\{(\beta_{ns}R)^2-n^2\}} \quad \text{for } n>0, \tag{32b}$$

where

$$\Psi_{is} = \frac{(\lambda_{ni}R)^3 J_n'(\lambda_{ni}R)}{(\beta_{ns}R)^4-(\lambda_{ni}R)^4}, \quad \Psi_{ks} = \frac{(\lambda_{nk}R)^3 J_n'(\lambda_{nk}R)}{(\beta_{ns}R)^4-(\lambda_{nk}R)^4}, \quad i,k=1,2,\ldots,M. \tag{32c}$$

In Eqs. (32a,b), the sum of s must be stopped for numerical computation, at an integer value large enough to give the required accuracy.

The reference kinetic energy of the circular plate, as obtained by using the orthogonality of mode shapes, is presented:

$$T_p^* = \frac{\rho}{2}\,h\kappa_\theta \mathbf{q}^{\mathrm{T}}\mathbf{Z}\mathbf{q}, \tag{33}$$

where $\mathbf{Z}$ is the $M \times M$ matrix given as

$$Z_{ik} = \delta_{ik}\int_0^R rW_{ni}W_{nk}\,\mathrm{d}r, \quad \delta_{ik}: \text{Kronecker delta}. \tag{34}$$

When Eq. (3) is inserted into Eq. (34) and the integration is carried out, one can obtain a simple expression:

$$Z_{ik} = R^2\{J_n(\lambda_{ni}R)\}^2\delta_{ik}. \tag{35}$$

The maximum potential energy of the plate can be computed as a sum of the kinetic energy of the dry eigen functions:

$$V_d = \frac{\kappa_\theta}{2} D \int_0^R \left((\nabla^2 w)^2 - 2(1-\mu)\left\{ (w_{,rr})\left(\frac{w_{,r}}{r} + \frac{w_{,\theta\theta}}{r^2}\right) - \left(\left[\frac{w_{,\theta}}{r}\right]_{,r}\right)^2 \right\} \right) r\,\mathrm{d}r. \tag{36}$$

As the first term $(\nabla^2 w)^2$ in Eq. (36) is identical to $\lambda_{ni}^4 w^2$, and the other terms of Eq. (36) are negligible compared with the first term, the maximum potential energy will be given by

$$V_d \approx \frac{\kappa_\theta}{2} D\mathbf{q}^{\mathrm{T}}\mathbf{P}\mathbf{q}, \tag{37}$$

where $\mathbf{P}$ is the $M \times M$ diagonal matrix given by

$$P_{ik} = (\lambda_{ni}R)^4\{J_n(\lambda_{ni}R)\}^2\delta_{ik}/R^2. \tag{38}$$

In Eq. (26), the correspondence between the reference total kinetic energy multiplied by its square circular frequency and the maximum potential energy of the same mode is used in order to find the coupled natural frequencies. Minimizing the Rayleigh quotient with respect to the unknown parameters q_m, the equation can be obtained:

$$\{D\mathbf{P} - \omega^2(\rho h\mathbf{Z} + \rho_o\mathbf{G})\}\mathbf{q} = \{0\}. \tag{39}$$

Determinant of Eq. (39) must vanish to obtain the non-trivial solution, and the natural frequency ω in the wet condition can be calculated. However, the solution of the problem cannot be obtained as a linear eigenvalue problem, so an iterative algorithm must be implemented.

3. Examples and discussion

3.1. Theoretical and finite element models

On the basis of the preceding analysis, in order to find the natural frequencies of a circular plate coupled with the radially bounded fluid by the cylindrical rigid wall, the determinant of the left side in Eq. (39) is calculated using a commercial software Mathcad [15]. The frequency equation derived in the preceding sections involves an infinite and a finite series of algebraic terms. In the theoretical calculation, the Bessel–Fourier expansion term s is set at 200 and the expanding term m for the admissible function is set at 40, which gives a converged solution. Since the solution of the problem cannot be obtained using the linear eigenvalue operating command of Mathcad, an iterative algorithm was created using programming operators. It could be achieved by starting from some assumed values of ω. For this calculation, first of all, these initial values were determined by considering the incompressible fluid case.

Additionally, in order to check the validity of the theory, a fluid-submerged circular plate was examined by finite element analysis using a commercial computer code, ANSYS (release 6.1) [16]. The finite element model has the identical plate geometry, boundary conditions and material

properties used in the theoretical calculation. The plate is made of aluminum having a radius of 120 mm and a thickness of 2 mm. The total height of the rigid circular cylindrical container was 82 mm and the fluid region was divided into two regions; the upper fluid region with the height of 60 mm and the lower fluid region with the height of 20 mm. The physical properties of the plate and the fluid were as follows: Young's modulus = 69.0 GPa, Poisson's ratio = 0.3, plate mass density = 2700 kg/m^3, and fluid density = 1000 kg/m^3. The viscosity of the fluid was neglected in the theoretical calculation and the finite element analysis. Three cases of compressibility are considered in the finite element model; the Bulk moduli of the fluid are 2.2×10^8, 2.2×10^9, and 2.2×10^{10} Pa, which are equivalent to 469, 1483, 4690 m/s of the speed sound in the fluid medium by Eq. (40).

Finite element analysis using ANSYS was performed to obtain the natural frequencies of the circular plate submerged in the bounded fluid. For the finite element method (FEM) analysis, an axisymmetric model was constructed with axisymmetric harmonic fluid elements (FLUID81) and axisymmetric harmonic shell elements (SHELL61) as illustrated in Fig. 2. The fluid element 'FLUID81' with four nodes has three degrees of freedom at each node. The shell element 'SHELL61' with two nodes has four degrees of freedom. The upper and lower fluid regions were divided into a number of fluid elements and the plate was also meshed with shell elements. The nodes of the fluid elements at $r = 0$ were constrained in the radial direction only. On the other hand, the fluid movement at $r = R$, namely along the rigid container wall, was restricted to the radial direction. The fluid cannot move in the vertical direction at $x = H_1$ and $x = H_2$ because of the impermeable rigid top and bottom walls. The vertical displacement of the fluid element nodes adjacent to each surface of the wetted circular plate coincided with those of the plate so that the finite element model could simulate Eqs. (15a) and (15b). The circular plate was divided into 48 axisymmetric shell elements of the same size. The upper fluid region of the finite element model consisted of 1152 (24×48) fluid elements, and the lower fluid region was meshed with 384 (8×48) fluid elements as illustrated in Fig. 2. A clamped boundary condition along the plate edge was applied in the finite element model. The natural frequencies of the first 50 modes between 30

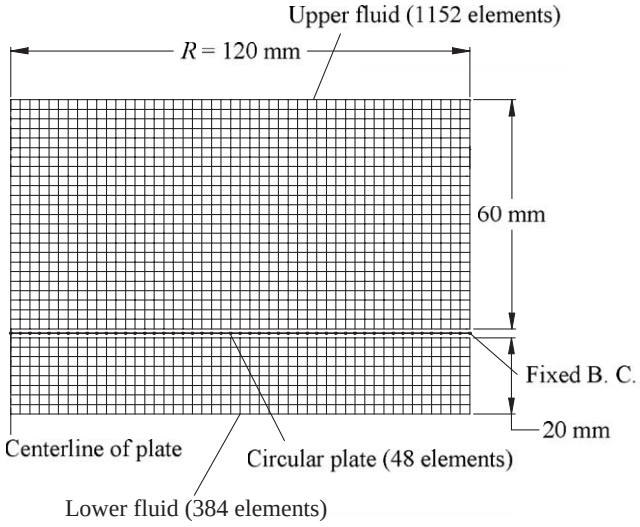

Fig. 2. Axisymmetric finite element model of a circular plate submerged in a fluid-filled rigid cylindrical container.

and 12000 Hz were extracted for each nodal diameter. In the finite element modal analysis, some pure fluid motion modes were detected when the lower frequency limit to be considered was less than that of the fluid motion modes, because the bulk modulus of the elasticity of water was taken into account. All the fluid modes without the structural motion were ignored in the finite element analysis and the frequency of these modes was usually lower than that of the fluid-coupled structural vibration modes. Therefore, the lower frequency limit was set at 30 Hz in order to avoid extracting the fluid motion modes. In the finite element analysis, the Block Lanczos-iteration extraction technique was used for obtaining the eigenvalue and eigenvector.

3.2. Theoretical and finite element results

The wet natural frequencies of the plate are listed in Tables 1–3 for the several bulk moduli, where the symbol m' represents the serial number in the radial direction for each fixed nodal diameter n. Table 1 shows the natural frequencies from the finite element analysis and the

Table 1
Fluid-coupled natural frequency (Hz) of a circular plate submerged in a fluid-filled rigid container with $H_1 = 60$ mm and $H_2 = 20$ mm , $B = 2.2 \times 10^8$ Pa

m'	Method	Number of nodal diameters (n)					
		0	1	2	3	4	5
	FEM (Hz)	—	122.7	294.1	523.5	809.2	1150.3
0	CO (Hz)[a]	—	122.8	294.2	523.6	809.4	1150.8
	Discrepancy (%)[b]	—	−0.08	−0.03	−0.02	−0.02	−0.04
	FEM (Hz)	315.9	607.6	978.6	1418.2	1920.9	2482.9
1	CO (Hz)	315.9	607.1	977.9	1417.4	1920.1	2482.5
	Discrepancy (%)	0.00	0.08	0.07	0.06	0.04	0.02
	FEM (Hz)	1008.5	1495.3	2059.2	2687.9	3372.1	4100.6
2	CO (Hz)	1007.3	1493.2	2055.6	2683.8	3367.8	4096.5
	Discrepancy (%)	0.12	0.14	0.17	0.15	0.13	0.10
	FEM (Hz)	2055.0	2625.6	3186.1	3752.0	4336.3	4942.2
3	CO (Hz)	2050.7	2619.4	3181.2	3748.5	4333.8	4940.5
	Discrepancy (%)	0.21	0.24	0.15	0.09	0.06	0.03
	FEM (Hz)	2826.3	3239.6	3833.9	4531.5	5268.8	6002.5
4	CO (Hz)	2822.9	3233.9	3825.4	4521.3	5258.2	5992.7
	Discrepancy (%)	0.12	0.18	0.22	0.22	0.20	0.16
	FEM (Hz)	3499.9	4230.4	4964.4	5700.4	6443.1	7080.0
5	CO (Hz)	3494.1	4223.0	4957.5	5693.4	6439.8	7073.8
	Discrepancy (%)	0.16	0.17	0.14	0.12	0.05	0.09

Note:
[a]CO : Theoretical result based on the compressible fluid.
[b]Discrepancy (%) = (FEM–CO) X 100 / FEM.

Table 2
Fluid-coupled natural frequency (Hz) of a circular plate submerged in a fluid-filled rigid container with $H_1 = 60$ mm and $H_2 = 20$ mm, $B = 2.2 \times 10^9$ Pa

m'	Method	Number of nodal diameters (n)					
		0	1	2	3	4	5
0	FEM (Hz)	—	123.2	296.1	528.5	819.3	1168.6
	IC (Hz)[a]	—	123.3	296.4	529.1	820.7	1171.2
	CO (Hz)[b]	—	123.2	296.1	528.6	819.6	1169.2
	Discrepancy (%)[c]	—	0.00	0.00	−- 0.02	−0.04	- 0.05
1	FEM (Hz)	319.6	618.9	1002.4	1459.9	1987.8	2584.5
	IC (Hz)	376.6	619.7	1004.2	1463.6	1994.1	594.8
	CO (Hz)	319.6	618.4	1001.6	1459.1	1987.1	2584.2
	Discrepancy (%)	0.00	0.08	0.08	0.05	0.04	0.01
2	FEM (Hz)	1042.1	1567.2	2182.4	2880.1	3655.9	4507.7
	IC (Hz)	1086.7	1571.3	2190.1	2892.7	3675.2	4535.8
	CO (Hz)	1041.0	1564.1	2178.3	2875.4	3650.9	4502.7
	Discrepancy (%)	0.11	0.20	0.19	0.16	0.14	0.11
3	FEM (Hz)	2231.0	2999.3	3861.3	4811.4	5845.2	6959.7
	IC (Hz)	2275.1	3014.5	3885.3	4846.3	5893.6	7025.3
	CO (Hz)	2225.8	2989.2	3848.7	4797.0	5829.4	6943.2
	Discrepancy (%)	0.23	0.34	0.33	0.30	0.27	0.24
4	FEM (Hz)	3912.5	4934.0	6051.5	7262.1	8560.5	9942.7
	IC (Hz)	3973.2	4979.5	6116.6	7348.8	8672.1	10084.6
	CO (Hz)	3897.6	4909.4	6022.1	7229.0	8524.3	9904.3
	Discrepancy (%)	0.38	0.50	0.49	0.46	0.42	0.39
5	FEM (Hz)	6086.7	7351.6	8713.4	10180.0	11742.8	13392.9
	IC (Hz)	6207.4	7491.6	8906.7	10420.4	12029.1	13730.2
	CO (Hz)	6056.8	7303.1	8658.2	10119.2	11676.9	13322.6
	Discrepancy (%)	0.49	0.66	0.63	0.60	0.56	0.52

Note: IC
[a]Theoretical result based on the compressible fluid.
[b]CO : Theoretical result based on the compressible fluid.
[c]Discrepancy (%) = (FEM–CO) X 100 / FEM.

theoretical calculation based on the assumption of a compressible fluid in the mode range of $0 \leqslant n \leqslant 5$ and $0 < m' < 5$. The mode with $n = 0$ and $m' = 0$ cannot appear because the particular mode violates the fluid volume conservation. As the fluid bulk modulus of 2.2×10^8 Pa is equivalent to 10% of the water bulk modulus in room temperature, the fluid may act as a compressible fluid. It was found that the theoretical natural frequencies excellently agree with the finite element results within a ±0.3% discrepancy range as shown in Table 1. The theoretical natural frequencies based on the compressible fluid is slightly less than the FEM results for $m' > 0$, but it was reversed for $m' = 0$. A further demonstration is given in Table 2 which shows the

natural frequencies obtained by the finite element analysis and the theoretical calculation in the same mode range. The real bulk modulus of water in room temperature was used in the finite element analysis, which is equivalent to 2.2×10^9 Pa, and the theoretical calculations were carried out for both cases; one is based on the incompressible fluid assumption, and the other the compressible fluid assumption. The difference between the two cases is negligible for $n>0$ as shown in Table 2. Hence, the water can be considered as an incompressible fluid in the range of a physical scale of the example for $n>0$. Meanwhile, it was shown that there is a remarkable difference between the two cases for $n=0$ because the lower radial modes with the zero nodal line are susceptible to the fluid volume conservation requirement.

Clearly, the potential energy of a compressible fluid tends to reduce the natural frequency of the structure like the kinetic energy of the fluid. For $n=0$, therefore, the assumption of an incompressible fluid causes an overestimation of the natural frequencies compared to the finite element results which are based upon the compressible fluid assumption. Especially, the first

Table 3
Fluid-coupled natural frequency (Hz) of a circular plate submerged in a fluid-filled rigid container with $H_1 = 60$ mm and $H_2 = 20$ mm, $B = 2.2x10^{10}$ Pa

m'	Method	Number of nodal diameters (n)					
		0	1	2	3	4	5
	FEM (Hz)	—	123.3	296.3	529.0	820.3	1170.4
0	IC (Hz)[a]	—	123.3	296.4	529.1	820.7	1171.2
	Discrepancy (%)[b]	—	0.00	0.03	0.02	0.05	0.07
	FEM (Hz)	320.0	620.0	1004.7	1464.0	1994.1	2594.0
1	IC (Hz)	376.6	619.7	1004.2	1463.6	1994.1	2594.8
	Discrepancy (%)	−17.68	−0.05	−0.05	−0.03	0.00	0.03
	FEM (Hz)	1045.4	1573.7	2193.1	2895.8	3677.9	4537.5
2	IC (Hz)	1086.7	1571.3	2190.1	2892.7	3675.2	4535.8
	Discrepancy (%)	−3.95	−0.15	−0.14	−0.11	−0.07	−0.04
	FEM (Hz)	2244.7	3022.3	3894.5	4856.1	5903.3	7033.9
3	IC (Hz)	2275.1	3014.5	3885.3	4846.3	5893.6	7025.3
	Discrepancy (%)	−1.35	−0.26	−0.23	−0.20	−0.16	−0.12
	FEM (Hz)	3954.4	4998.3	6138.2	7371.8	8695.5	10106.8
4	IC (Hz)	3973.2	4979.5	6116.6	7348.8	8672.1	10084.6
	Discrepancy (%)	−0.47	−0.38	−0.35	−0.31	−0.27	−0.22
	FEM (Hz)	6205.0	7529.5	8949.0	10465.2	12074.6	13774.7
5	IC (Hz)	6207.4	7491.6	8906.7	10420.4	12029.1	13730.2
	Discrepancy (%)	−0.04	−0.50	−0.47	−0.43	−0.38	−0.32

Note:
[a]IC : Theoretical result based on the compressible fluid.
[b]Discrepancy (%) = (FEM–CO) X 100 / FEM.

natural frequency ($n = 0$ and $m' = 1$) is 319.6 Hz in the finite element analysis, and it is equivalent to 379.6 Hz in the theoretical calculation based on the incompressible fluid assumption as listed in Table 2. The discrepancy between them is as much as −17.8%. The serious discrepancy also can be observed for $n = 0$ in the case of $B = 2.2 \times 10^{10}$ Pa, which is equivalent to ten times of water bulk modulus, as shown in Table 3. However, the theoretical formulation with the compressible fluid assumption could reduce drastically the discrepancy to nearly zero. It demonstrates that the incompressible fluid assumption for water sometimes can produce an unexpected error for the lower modes with $n = 0$, but the error can be overcome by the formulation founded on the compressible fluid assumption. For a further investigation, the theoretical calculation based on the incompressible fluid assumption was fulfilled and was listed in Table 3 for when the fluid bulk modulus is equivalent to 10 times that of the water. The results also showed that the incompressible fluid assumption is still valid for $n > 0$, but it is invalid for $n = 0$. The behavior of

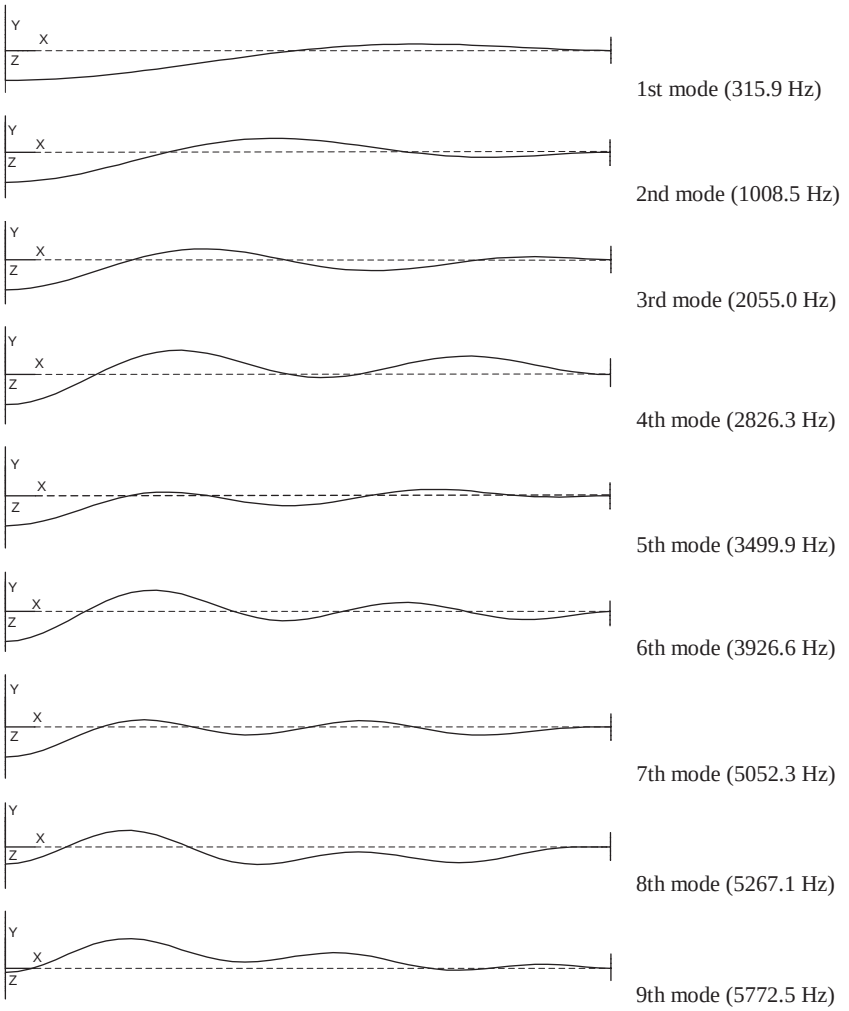

Fig. 3. Mode shapes of a circular plate submerged in a compressible fluid with $n = 0$ and $B = 2.2 \times 10^8$ Pa.

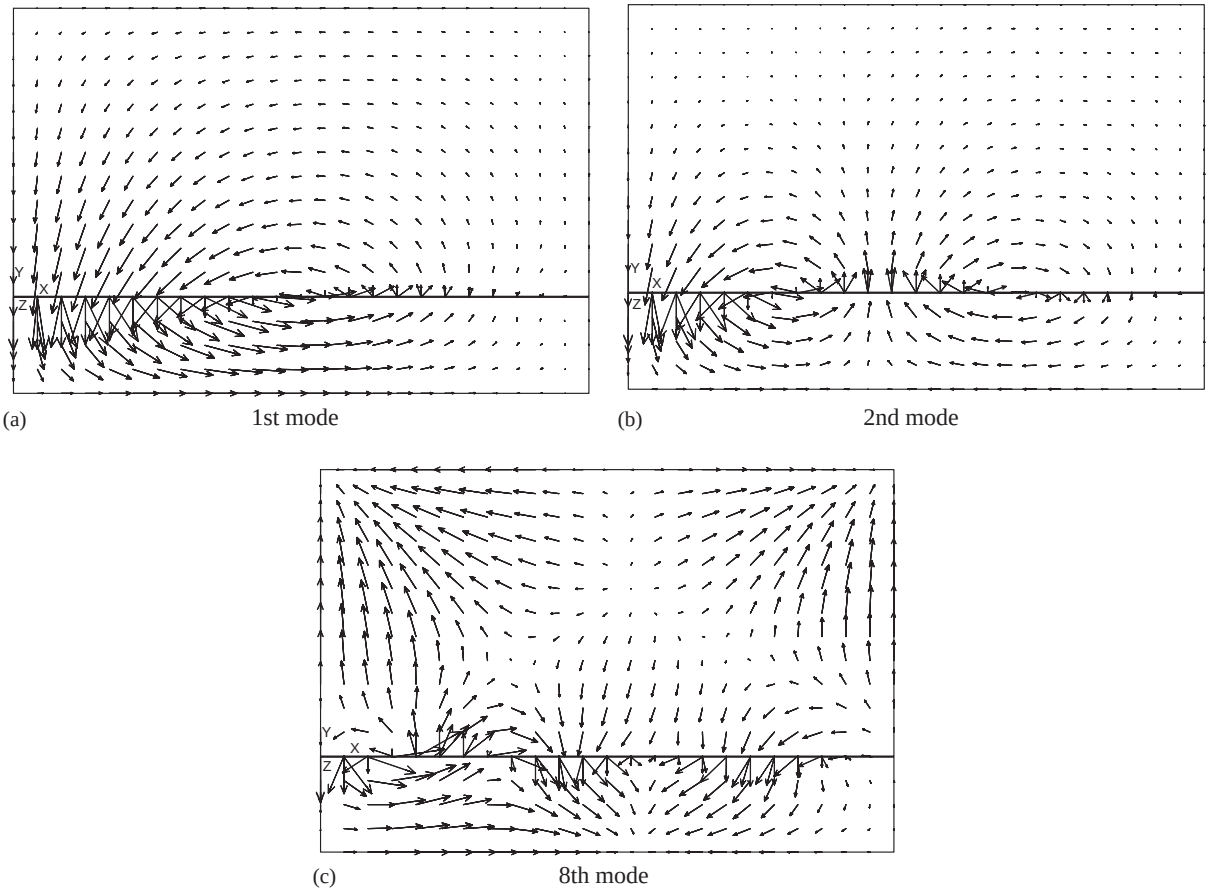

Fig. 4. Displacement vector plots of typical mode shapes with $n = 0$ and $B = 2.2 \times 10^8$ Pa.

the frequency loci resembles that of the out-of-phase mode for the two identical circular plates coupled with water as delineated in Ref. [12]. That is to say, the maximum discrepancy between the theoretical and FEM results appeared at the mode with $n = 0$, $m' = 1$, since the theory was formulated by an assumption of an incompressible fluid.

It is well known that the nodal circle increases one by one for a circular plate in incompressible fluid or in air, when the mode number m' increases for the fixed nodal diameter n. However, when the bulk modulus of the fluid is 2.2×10^8 Pa, which is equivalent to 10% of the water bulk modulus, the fluid acts as a compressible fluid. The mode number m' does not indicate the number of nodal circles any more as shown inFig. 3. Both the 5th and 6th modes have four nodal circles, but they have different mode shapes and natural frequencies. Sometimes the crossing point of the nodal circles changes to the saddle point as shown in the 8th and 9th modes of Fig. 3. It is interesting to observe that several modes can appear for the fixed nodal circle and nodal diameter for the compressible fluid owing to the compressibility of the fluid. As indicated in the vector plots of Fig. 4, a group of similar neighboring mode shapes can be developed due to the fluid surge induced by the fluid compressibility. As shown in the vector plots of Fig. 4, the first and second

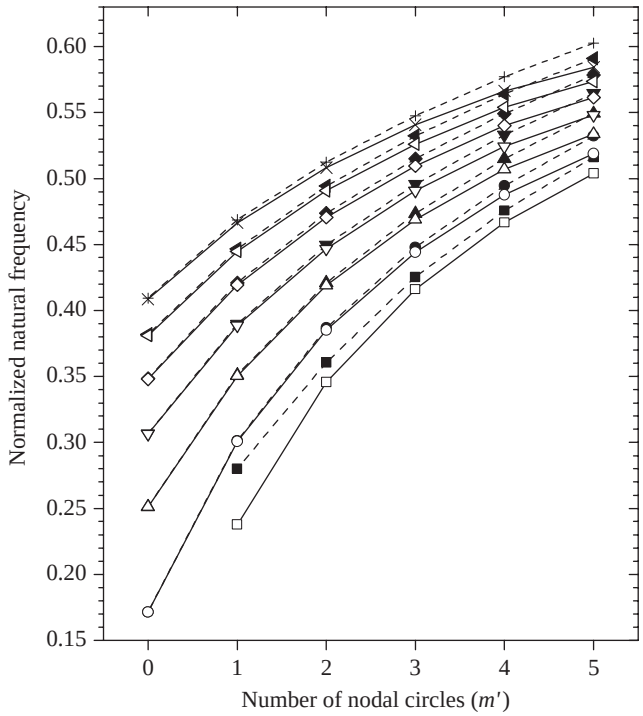

Fig. 5. Normalized natural frequency with respect to number of nodal circles for water with $H_1 = 60$ mm and $H_2 = 20$ mm: incompressible fluid case; – – ■ – –, $n = 0$; – – ● – –, $n = 1$; – – ▲ – –, $n = 2$; – – ▼ – –, $n = 3$; – – ◆ – –, $n = 4$; – – ◀ – –, $n = 5$; – – + – –, $n = 6$: compressible fluid case, $B = 2.2 \times 10^9$ Pa; —□—, $n = 0$; —○—, $n = 1$; —△—, $n = 2$; —▽—, $n = 3$; —◇—, $n = 4$; —◁—, $n = 5$; —×—, $n = 6$.

modes of the circular plate submerged in the compressible fluid indicate a very similar fluid displacement vector pattern to that of the incompressible fluid case. The fluid movement is dominant near the plate, and the fluid movement far from the anti-node of the plate is negligible. This is the typical displacement pattern of an elastic structure in an incompressible fluid medium. However, the fluid displacement vector plot of the eighth mode in Fig. 4 is different from that of the fluid movement of the equivalent mode of the plate submerged in an incompressible fluid medium. The flow surge at the fluid region far from the anti-node is induced by the compressibility of the fluid.

It is well known that the natural frequency of the plate in contact with an incompressible fluid is always less than the natural frequency of the corresponding dry mode, due to the contribution of the hydrodynamic mass. Hence, the normalized natural frequencies, defined as the natural frequency of a structure in contact with an incompressible fluid divided by the corresponding natural frequency of the structure in air, always lies between unity and zero. As shown in Figs. 5 and 6, the normalized natural frequency gradually increases with the number of nodal diameters or nodal circles by virtue of the separation of the fluid flow direction, because an increase in the number of nodal diameters (n) or nodal circles (m') can gradually restrict the movement of the incompressible or compressible fluid and reduces the hydrodynamic mass.

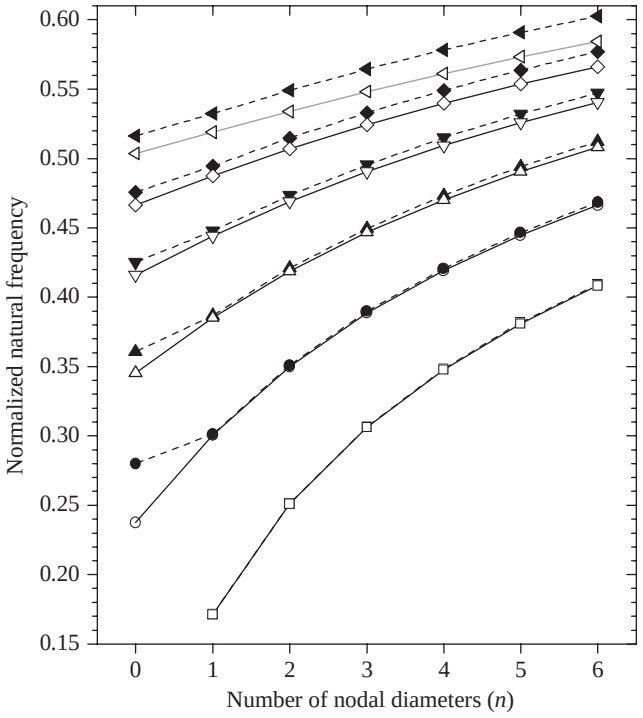

Fig. 6. Normalized natural frequency with respect to number of nodal diameters for water with $H_1 = 60$ mm and $H_2 = 20$ mm: incompressible fluid case; – – ■ – –, $m' = 0$; – – ● – –, $m' = 1$; – – ▲ – –, $m' = 2$; – – ▼ – –, $m' = 3$; – – ◆ – –, $m' = 4$; – – ◀ – –, $m' = 5$: compressible fluid case, $B = 2.2 \times 10^9$ Pa; —□—, $m' = 0$; —◯—, $m' = 1$; —△—, $m' = 2$; —▽—, $m' = 3$; —◇—, $m' = 4$; —◁—, $m' = 5$.

3.3. *Effect of fluid compressibility*

The fluid compressibility should be considered if the fluid is a two-phase fluid or some oils. The fluid compressibility is defined as a fluid bulk modulus or sound speed in a fluid medium.

$$\mathbf{B} = \rho_o c^2. \tag{40}$$

The natural frequency of the plate decreases with an increase of fluid compressibility as shown in Tables 1–3. Especially, the compressibility effect on the natural frequency is dominant at the higher modes. The natural frequency of the mode with $n = 1$ and $m' = 3$ shifts from 2625.6 to 2999.3 Hz when the bulk modulus of the fluid changes 2.2×10^8 to 2.2×10^9 Pa. However, the frequency difference is less than 1.0 Hz for the first mode with $n = 1$ and $m' = 0$. In the mode shapes of the plate submerged in the compressible fluid with $B = 2.2 \times 10^8$ Pa and $n = 0$, as illustrated in Fig. 3, it was observed that the normal mode shapes appear at the lower modes and the abnormal mode shapes follow according to increasing the mode numbers for the fixed nodal diameter, where the abnormal mode shapes mean that the distorted mode shapes by the fluid surge phenomena due to the fluid compressibility. From this point of view, the first three and 6th

modes in the Fig. 3 are the normal modes, but the 4th, 5th, 7th, 8th, and 9th modes are the abnormal modes developed by the fluid compressibility. The normal mode shapes as shown in Fig. 4(a) and (b) indicate that the fluid displacement vector scale is prominent near the plate. However far from the plate, the magnitude of the fluid displacement vector is gradually diminished. In the abnormal mode case, the magnitude of fluid displacement vector does not depend any more on the distance from the plate as shown in the 8th mode of Fig. 4(c).

3.4. Effect of offcenter distance

The circular plate can be fixed along any location in the rigid circular cylindrical container. In order to investigate the effect of the plate location in the container, the offcenter factor is defined as

$$\eta = \frac{|H_1 - H_2|}{H_1 + H_2}. \tag{41}$$

Figs. 7and 8 show the effect of the offcenter distance from the center location of the rigid cylindrical vessel. The offcenter direction may be upward or downward, but the direction cannot affect the modal parameter of the system. As for increasing the offcenter distance, the normalized

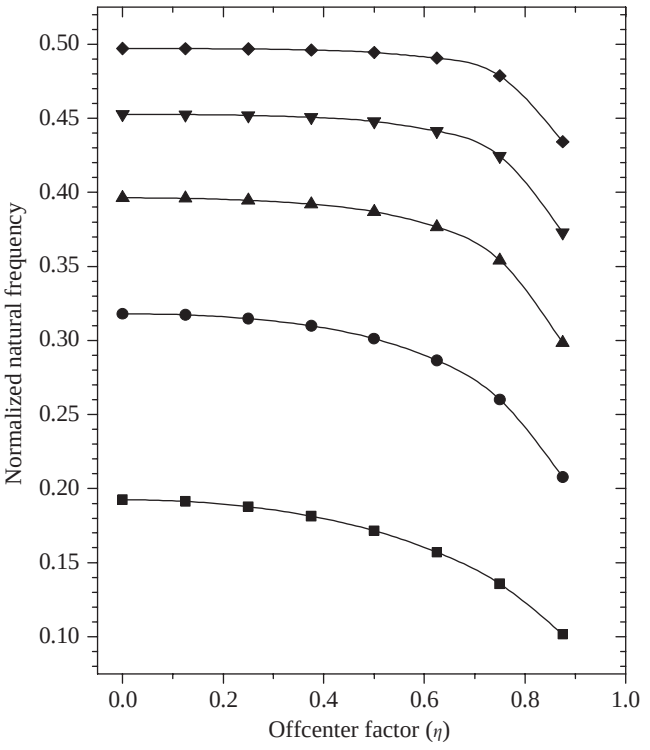

Fig. 7. Offcenter effect on normalized natural frequency for incompressible fluid with $n = 1$; —■—, $m' = 0$; —●—, $m' = 1$; —▲—, $m' = 2$; —▼—, $m' = 3$; —◆—, $m' = 4$.

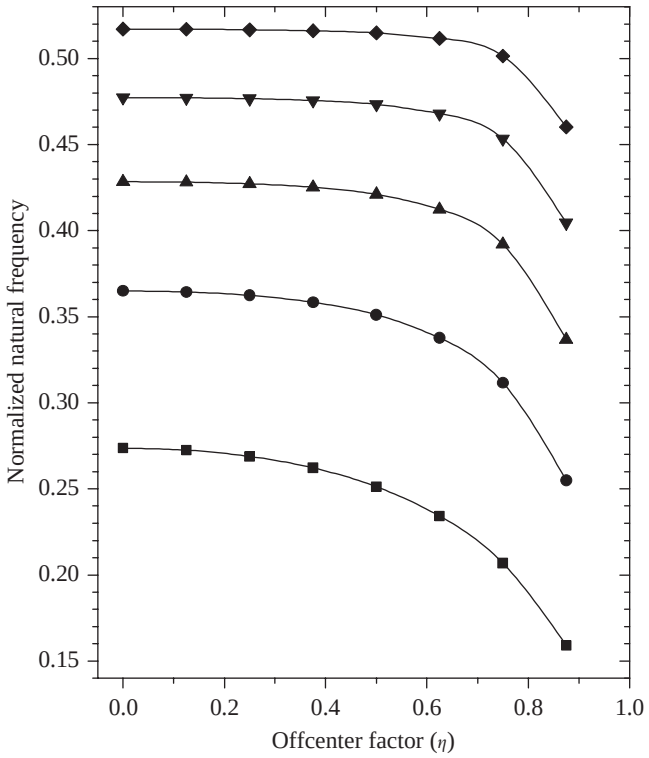

Fig. 8. Offcenter effect on normalized natural frequency for incompressible fluid with $n = 2$; —■—, $m' = 0$; —●—, $m' = 1$; —▲—, $m' = 2$; —▼—, $m' = 3$; —◆—, $m' = 4$.

natural frequencies decrease as illustrated in Figs. 7 and 8. Especially, when the offcenter distance approaches unity, the normalized natural frequencies abruptly decrease. This means that the natural frequencies drastically decrease when the plate approaches the cylindrical container bottom or top surfaces. This shows that the natural frequencies depend on the distance between the structures although the amount of fluid remains.

4. Conclusions

An analytical method to estimate the natural frequencies of a circular plate coupled with a compressible fluid was developed by the Rayleigh–Ritz method and the finite Fourier–Bessel series expansion method. It was verified that the theoretical approach based on the compressible fluid assumption can predict the coupled natural frequencies exactly. It was found that the normalized natural frequencies drastically decrease, when the offcenter distance approaches unity. It was clarified that the incompressible fluid assumption for water sometimes can produce an unexpected error for the lower modes with $n = 0$, and the error can be reduced by the theoretical formulation based on the compressible fluid assumption. Several additional abnormal modes were observed at the circular plate submerged in a compressible fluid due to the fluid surge. It was also

found that the normalized natural frequencies monotonically increase, when the number of diametrical or circular modes increases for both the incompressible and compressible cases, and the natural frequencies drastically decrease when the plate approaches the rigid cylindrical container's bottom or top surfaces.

References

[1] M.K. Kwak, Vibration of circular plates in contact with water, *Journal of Applied Mechanics* 58 (1991) 480–483.
[2] M.K. Kwak, K.C. Kim, Axisymmetric vibration of circular plates in contact with fluid, *Journal of Sound and Vibration* 146 (1991) 381–389.
[3] M.K. Kwak, S.B. Han, Effect of fluid depth on the hydroelastic vibration of free-edge circular plate, *Journal of Sound and Vibration* 230 (2000) 171–185.
[4] M. Amabili, Effect of finite fluid depth on the hydroelastic vibrations of circular and annular plates, *Journal of Sound and Vibration* 193 (1996) 909–925.
[5] M. Amabili, M.K. Kwak, Free vibration of circular plates coupled with liquids: revising the Lamb problem, *Journal of Fluids and Structures* 10 (1996) 743–761.
[6] M. Amabili, M.K. Kwak, Vibration of circular plates on a free fluid surface: effect of surface waves, *Journal of Sound and Vibration* 1999 (226) 407–424.
[7] M. Chiba, Axisymmetric free hydroelastic vibration of a flexural bottom plate in a cylindrical tank supported on an elastic foundation, *Journal of Sound and Vibration* 169 (1994) 387–394.
[8] H.F. Bauer, Coupled frequencies of a liquid in a circular cylindrical container with elastic liquid surface cover, *Journal of Sound and Vibration* 180 (1995) 689–704.
[9] M. Amabili, Vibrations of circular plates resting on a sloshing liquid: solution of the fully coupled problem, *Journal of Sound and Vibration* 245 (2001) 261–283.
[10] M. Amabili, G. Dalpiaz, C. Santolini, Free-edge circular plates vibrating in water, *Modal Analysis: The International Journal of Analytical and Experimental Modal Analysis* 10 (1995) 187–202.
[11] Y.K. Cheung, D. Zhou, Hydroelastic vibration of a circular container bottom plate using the Galerkin method, *Journal of Fluids and Structures* 16 (2002) 561–580.
[12] K.H. Jeong, Free vibration of two identical circular plates coupled with bounded fluid, *Journal of Sound and Vibration* 260 (2003) 653–670.
[13] F. Zhu, Rayleigh quotients for coupled free vibration, *Journal of Sound and Vibration* 171 (1994) 641–649.
[14] M. Amabili, Eigenvalue problems for vibrating structures coupled with quiescent fluids with free surface, *Journal of Sound and Vibration* 231 (2000) 79–97.
[15] Mathcad User's Guide-Mathcad 2000 Professional, MathSoft Inc., Cambridge, MA, USA, 1999.
[16] P. Kohnke, ANSYS theory reference, ANSYS elements reference, ANSYS command reference, release 5.4, SAS IP, Inc. 1997.